Nano-Confinement Induced Chain Alignment in Ordered P3HT Nanostructures Defined by Nanoimprint Lithography

Mukti Aryal, Krutarth Trivedi, and Wenchuang (Walter) Hu*

Department of Electrical Engineering, The University of Texas at Dallas, Richardson, Texas

ABSTRACT Control of polymer morphology and chain orientation is of great importance in organic solar cells and field effect transistors (OFETs). Here we report the use of nanoimprint lithography to fabricate large-area, high-density, and ordered nanostructures in conjugated polymer poly(3-hexylthiophene) or P3HT, and also to simultaneously control 3D chain alignment within these P3HT nanostructures. Out-of-plane and in-plane grazing incident X-ray diffraction were used to determine the chain orientation in the imprinted P3HT nanostructures, which shows a strong dependence on their geometry (gratings or pillars). Vertical chain alignment was observed in both nanogratings and nanopillars, indicating strong potential to improve charge transport and optical properties for solar cells in comparison to bulk heterojunction structure. For P3HT nanogratings, $\pi-\pi$ stacking along the grating direction with an angular distribution of $\pm 20°$ was found, which is favorable for OFETs. We propose the chain alignment is induced by the nanoconfinement during nanoimprinting via $\pi-\pi$ interaction and hydrophobic interaction between polymer chain and mold surfaces.

KEYWORDS: polymer chain alignment · nanostructures · poly(3-hexylthiophene) or P3HT · organic solar cells · organic field effect transistors

During the past decade, conjugated polymers have emerged as cost-effective functional materials for organic electronic devices such as solar cells[1,2] and field effect transistors (FETs).[3,4] In organic devices, polymer morphology (size and shape of polymer nanostructures or phases) and chain orientation or crystallinity have been shown to have strong effects on charge-carrier mobility and overall device performance.[5,6] This is because charge transport in conjugated polymer is anisotropic, resulting from electrons delocalized along the polymer backbone and the overlap of π-orbitals.[7] For example, charge mobility of poly(3-hexylthiophene) (P3HT) along the $\pi-\pi$ stacking and backbone direction can be higher than 0.1 $cm^2/V \cdot s$, while being several orders of magnitude lower along the insulating side chains.[8,9] Consequently, charge transport, mobility, and even optical properties across the active layer of a device can be significantly affected by ordering and crystallinity of P3HT.[8−11] In addition to chain orientation, control over polymer morphology can be important for device performance as well. For example, in bulk heterojunction (BHJ) solar cell structures, control of nanomorphology of the heterojunction plays a critical role in exciton dissociation and charge transport.[5] In most cases, chain alignment and morphology are interrelated and it is difficult to control both factors simultaneously and favorably. In BHJ solar cells, the hole mobility is just on the order of 10^{-4} $cm^2/V \cdot s$, which is attributed to both random chain alignment and overlapping phase morphology.[5,10,12]

Several techniques have been reported to promote nanoscale phase separation, polymer crystallization, and chain alignment in bulk heterojunction solar cells and FETs. Studies suggest polymer chain alignment and crystallization can be controlled to some extent by spincoating techniques,[13] solution concentration, and composition, drying process,[5,14] and surface modification.[9,15,16] Processing techniques such as nanorubbing,[17,18] electrospinning,[19] and nanoimprint lithography[20−23] have been attempted to control polymer morphology and improve crystallinity/orientation of P3HT. These techniques have achieved some degree of chain ordering, some of them leading to improved device performance. However, a comprehensive understanding of chain alignment in defined nanostructure morphologies remains unknown. Simultaneous control of polymer chain alignment and morphology is still a challenge.

Previously, we have demonstrated the use of nanoimprint lithography to define high-density nanopillars/pores in P3HT

*Address correspondence to walter.hu@utdallas.edu.

Received for review July 20, 2009 and accepted August 26, 2009.

Published online September 4, 2009.
10.1021/nn900831m CCC: $40.75

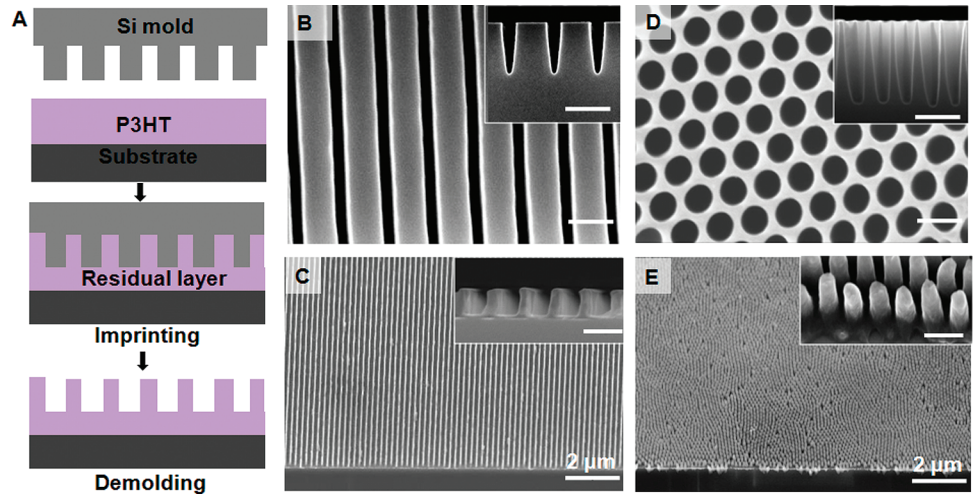

Figure 1. (A) Schematic of nanoimprinting process. (B) SEM top view of Si nanograting molds of 200 nm in pitch, 65 nm in width, and 200 nm in depth. Inset image shows the cross section of the mold; (C) SEM 45° tilted view of imprinted P3HT nanogratings of the same dimensions as the mold. The residual layer is about 20 nm and inset image shows the cross section of the grating. (D) Nanoporous Si mold with hexagonal pore array of 80 nm in diameter, 350 nm in height, and 100 nm in pitch. Inset image shows the cross section. (E) SEM 45° tilted view of the nanoimprinted hexagonal array of nanopillars of 80 nm in diameter, 200−250 nm in height, and 100 nm in pitch. The residual layer is also about 20 nm. Scale bar is 200 nm unless otherwise specified.

and form vertically interdigitized bicontinuous heterojunction morphology for P3HT-fullerene derivative solar cells.[20] In this study, a similar process is used to make large-area P3HT nanostructures with different geometry, for example, gratings and pillars. We then show that the nanoimprinting process induces favorable chain alignment in all three-dimensions in these P3HT nanostructures, which is determined primarily by the geometry of nanoconfinement during nanoimprint and the surface properties of the mold. Interestingly, such 3D chain configuration is desirable for both solar cell and FET applications.

RESULTS AND DISCUSSION

In our experiments, regioregular or RR P3HT was used to prepare thin films of 80 nm thickness on a Si substrate and baked to drive out the solvent. As shown in Figure 1A, the film was nanoimprinted with Si nanograting (unpublished data) and nanoporous[20] molds that were prepared previously. The molds were treated with an antiadhesion monolayer, 1*H*,1*H*,2*H*,2*H*-perfluorodecyltrichlorosilane (FDTS). The nanograting mold consists of 200 nm deep, 65 nm wide trenches with a pitch of 200 nm (Figure 1B) while the nanoporous mold consists of a hexagonal array of 350 nm deep nanopores with 80 nm diameter (Figure 1D). Selection of the imprint conditions is strongly related to physical properties of the P3HT polymer. Typically, polymer is imprinted at 20−50 °C above its glass transition temperature (T_g). The T_g of P3HT is around 67 °C.[24] However imprinting at 20−50 °C higher than this temperature has resulted in poor polymer filling. This is because the crystallization occurs at this temperature range. The crystallization temperature (T_c) of P3HT ranges from 80 to 128 °C depending upon thermal history, cooling or heating rate and time.[25,26] In addition, P3HT does not have a well-defined T_g since it undergoes a twist-glass transition (twist of thiophene ring), which is a quasi-ordered phase transition of liquid crystals and plastic crystals.[24] With this understanding, the nanoimprint temperature was chosen at 170 °C, which is much higher than T_g and T_c but lower than the melting temperature T_m, so as to enhance P3HT chain disentanglement during polymer flow into nanocavities of the mold. The sample was cooled to 25 °C for demolding. The cooling process takes about 30 min, during which chain ordering and crystallization occur. Figure 1C shows SEM images of P3HT nanogratings with 200 nm period, 65 nm width, 200 nm height, and 20 nm residual layer, which are faithfully transferred from the mold. Figure 1E shows a hexagonal array of nanopores with diameter of 80 nm and height of 200−250 nm, and pitch of 100 nm. The optimized nanoimprint conditions have resulted in excellent polymer filling and pattern transfer fidelity.

P3HT crystallization and chain orientation were examined by out-of-plane and in-plane grazing incidence X-ray diffraction (GIXRD) measurement, which has previously been used to study film crystallinity.[15,16] Both out-of-plane (detector rotates vertically with respect to the sample) and in-plane (detector rotates horizontally with respect to the sample) GIXRD were obtained, as illustrated in Figure 2A. Figure 2A shows three typical P3HT chain orientations, edge-on, face-on, and vertical, where the lattice constants *a*, *b*, *c* are distance between backbones (~1.69 nm), π-stacking distance (~0.38 nm), and distance between side chains (~0.38 nm), respectively. In GIXRD, the orientation of the sample, with respect to the detector can be equally as important as with respect to the X-ray source. For P3HT

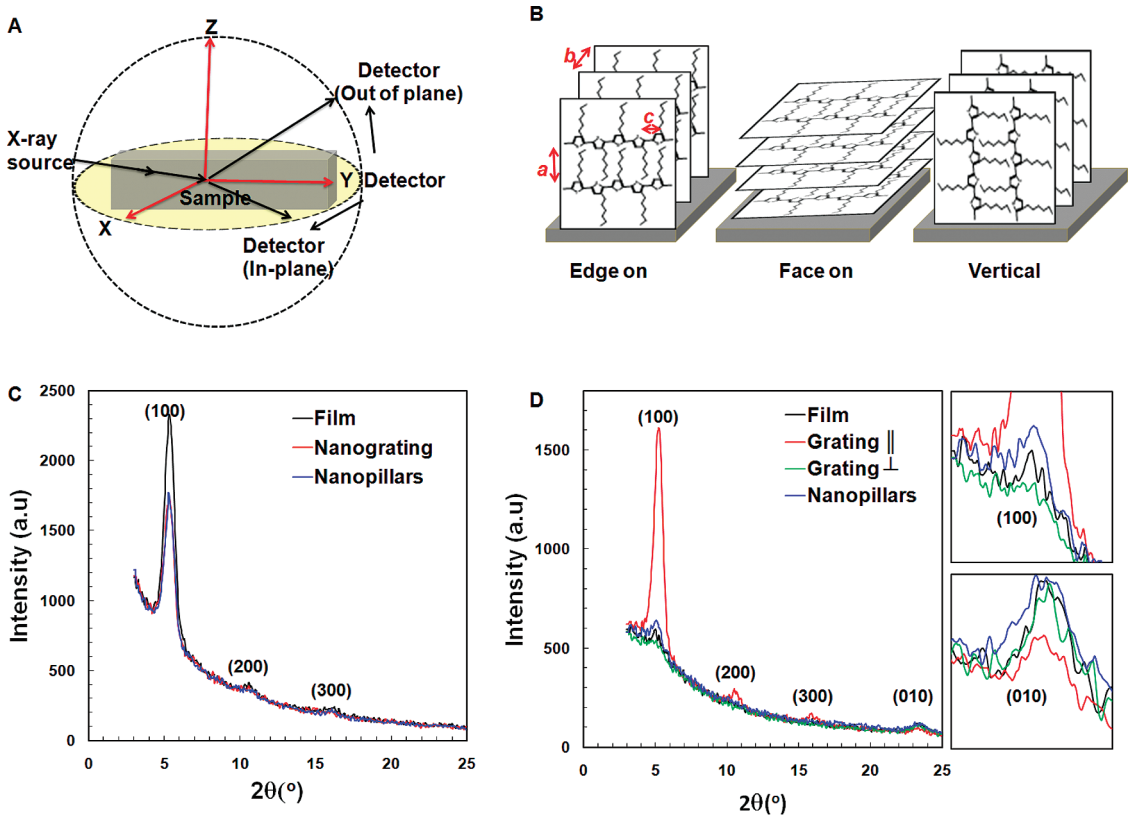

Figure 2. (A) Schematic of GIXRD setup for out-of-plane and in-plane measurements. (B) Schematic of edge-on, face-on, and vertical orientation of P3HT chains on surface. Out-of-plane and in-plane measurement are used to detect the lattice constants along *z*- axis and *x*-axis, respectively. (C) Out-of-plane GIXRD measurement graphs for the nanogratings, nanopillars, and unpatterned thin film samples. (D) In-plane GIXRD measurement graphs for all samples, where Grating ∥ and Grating ⊥ referred as measurements made with grating direction parallel and perpendicular to the direction of incident X-rays, respectively. The side figures show magnified views of the (100) peaks (top) and (010) peaks (bottom).

nanograting samples, in-plane GIXRD measurements were taken with grating direction along or parallel to the direction of incident X-rays (*y*-axis in Figure 2A, referred to as Grating∥) and with grating direction perpendicular to the direction of incident X-rays (*x*-axis in Figure 2A, referred to as Grating ⊥).

The out-of-plane GIXRD results of thin film, nanograting, and nanopillar samples are shown in Figure 2C. Large intensity (100) peaks at 5.2°, corresponding to lattice parameter *a*, were observed for all samples, suggesting dominance of edge-on chain orientation. In addition, the (010) peak at 23.4°, corresponding to the lattice parameter *b*, was not detected, indicating face-on chain orientation is not present (or negligible) in all samples. Comparatively, the (100) peak intensity for nanopillars and nanogratings was significantly reduced compared to thin film with similar volume, showing that edge-on dominance in the nanoimprinted P3HT is much reduced compared to unpatterned P3HT (thin film). This could be attributed to reordering of P3HT chains in the nanopillars and nanogratings during the nanoimprint process. We believe that the finite, lower intensity of this peak for patterned P3HT is resultant primarily from the residue layer of the nanoimprinted structures. This observation seems to be in agreement with a study by Cui *et al.*[22] The out-of-plane GIXRD results alone cannot provide a complete understanding of chain orientation of P3HT inside nanoimprinted structures. To gain a better understanding, in-plane XRD measurement was performed both along and perpendicular to the grating direction and results are shown in Figure 2D. The (100) peak was strongest for Grating ∥, while the same peak was weakest for Grating ⊥, indicating strong anisotropic chain orientation in nanoimprinted gratings. The strong (100) peak for Grating ∥, corresponding to lattice constant *a*, indicates that the only possible chain configurations in nanogratings are either face-on or vertical. However, the out-of-plane GIXRD measurement (Figure 2C) showed no face-on chain orientation (010 peak) in all samples. Therefore, this proves that chain orientation inside nanoimprinted gratings is, indeed, vertical. Furthermore, when the same nanograting samples were rotated by 90° for Grating ⊥, the (100) peak disappeared and (010) peak intensity increased, showing that for vertical chain orientation, the π-stacking is not randomly distributed in the *x*−*y* plane, but rather anisotropically aligned in one direction, that is, along the grating. With the combination of out-of-plane and in-plane GIXRD results, a complete picture of 3D P3HT chain configura-

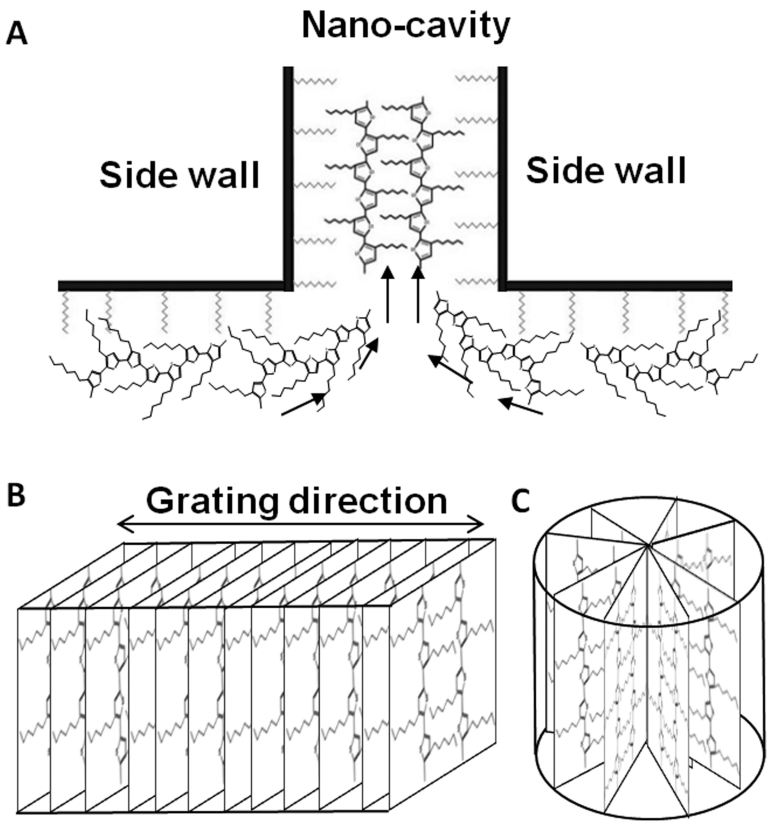

Figure 3. (A) Mechanism of P3HT chain alignment due to polymer flow and interaction between P3HT side chain and FDTS treated surface of the mold cavity during nanoimprinting; schematic of ideal structures of P3HT chain alignment in (B) nanograting and (C) nanopillars.

tion for nanogratings is obtained, that is, vertical backbone alignment with π-stacking along the grating direction as shown in Figure 3B (ideal case).

As for the nanopillar morphology, the (100) peak intensity in in-plane GIXRD (Figure 2D) was much lower than Grating ∥ but stronger than the unpatterned film as well as Grating ⊥, as shown in top magnified figure of Figure 2D. Similarly, the (010) peak for nanopillars is equally intense but broader compared to Grating ⊥ and unpatterned film (bottom magnified figure of Figure 2D). These observations indicate the presence of vertically oriented P3HT chains in the nanopillars. The measured signal for pillars did not change when the samples were rotated during measurements, indicating random or isotropic chain configuration in the $x-y$ plane. Figure 3C depicts the chain configuration in nanopillars (ideal case). Compared to nanograting and nanopillar samples, unpatterned P3HT film mostly exhibits edge-on chain orientation (Figure 2B) with random chain configuration in the $x-y$ plane, as evidenced by no peaks for the film in Figure 2D.

The above-mentioned results and analysis have shown that reordering of polymer chains is strongly affected by the geometry (gratings or pillars) of the mold, which confines and guides the flow of polymer to form P3HT nanostructures. While in-plane measurements (Grating ∥ and Grating ⊥) clearly prove that chains inside nanogratings are preferentially aligned in a certain direction, the two measurements do not reveal the variation in direction of chain alignment, with respect to grating direction. To measure the distribution of chain alignment directions, an azimuthal (ϕ) in-plane-prefer-orientation scan with the detector fixed at a 2θ angle of 5.2°, corresponding to (100) peak, was performed. As shown in Figure 4A, the sample was rotated from −40° to 115° in increments of 0.04° to scan a slew of directions, including the Grating ∥ and Grating ⊥ cases, for the (100) peak. Figure 4B shows the (100) peak intensity with respect to nanograting sample rotation (only −30° to 30° is shown). As expected, a peak maximum was observed when the incident beam is almost parallel to the nanograting direction (an angle of ∼3°, likely due to alignment error), which agrees with Grating ∥ data in Figure 2D. As seen in Figure 4B, the distribution has a width of ±20°, indicating the chain alignment (π stacking) has a finite variation along the grating direction. We believe that this variation can be minimized with optimized nanoimprint conditions (*e.g.*, longer imprinting time), appropriate structural aspect ratio, and better quality polymer.

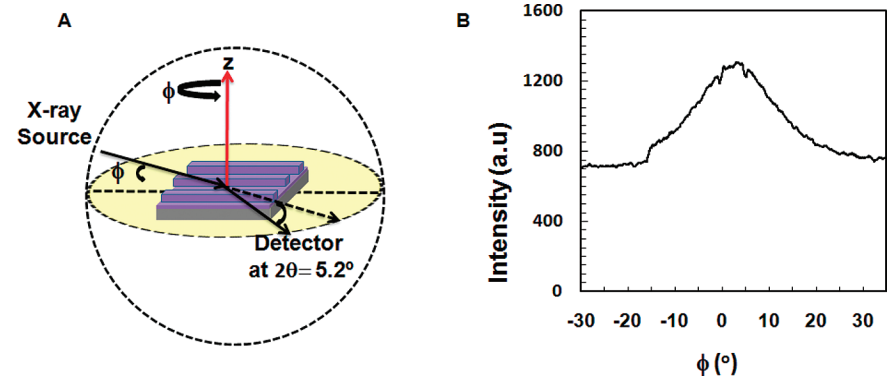

Figure 4. (A) Schematic of GIXRD setup for orientation measurement of nanograting sample. The detector is fixed at 2θ = 5.2° and the angle between X-ray incident beam and line grating varies when the thin film stage rotates though an angle ϕ. (B) Diffraction intensity *vs* ϕ for the detector fixed at 2θ = 5.2°.

This study provides a more complete understanding of polymer chain orientation in nanoimprinted structures and proves that the 3D configuration of P3HT chains can be controlled by geometry of nanostructures. Understanding of the fundamental mechanism that governs such unique chain orientation is important in applying this technique for controlling chain configuration in various applications. Previous studies have shown that reconfiguration of polymer chains can occur under various circumstances: (1) flow induced ordering,[27,28] flow in nanoscale dimensions,[29] flow at molten state,[30] flow under high pressure;[31] (2) hydrophobic interaction between side walls of the Si mold and P3HT side chains,[32] due to surface treatment effects;[15,16] (3) self-assembly of polymer due to side chain−side chain interaction and $\pi-\pi$ interaction.[15,16,33] These studies prove polymer chain ordering can occur during reflow in the viscoelastic state and such ordering can be strongly affected or even induced by the surfaces that the polymer contacts and the direction in which it flows. During the nanoimprint process, polymer flows into the nanocavities of the mold (gratings, pillars), under applied heat and pressure. As this process continues, polymer chains align along the flow direction, which was observed for the liquid crystalline and amorphous polymers.[34] The P3HT side chain interactions and the effect of hydrophobic mold surface add an extra feature for the 3D configuration of the chains for this polymer. We believe during our nanoimprint process (~170 °C) molecular chains rotate around the polymer backbone and its hydrophobic side chains interact with and turn toward the hydrophobic sidewalls of the mold (treated with hydrophobic FDTS), as shown in Figure 3A. This preferential chain alignment on surfaces of different surface energy has been shown in previous studies.[15,16] Thus, crystallization begins when this effect is cascaded throughout the imprinted P3HT. Studies have shown this directed organization can go up to tens of nanometers (~50 nm) for thin film P3HT contacting a substrate.[15] For imprinting, P3HT is confined in the mold cavity (at least two walls), this range should be at least doubled. This self-organization range may depend on the surface properties of the substrate, polymer, imprint time, and temperature. Final chain configuration is formed as temperature is reduced for demolding, likely resulting in comblike polymeric structures (Figure 3A). The possible comblike segments are ordered in a parallel lamella-type stack with interdigitized alkyl side chains to achieve maximum van der Waals interactions.[33] This mechanism, based on $\pi-\pi$ interchain interactions and side chain hydrophobic interactions with FDTS treated mold walls, can explain the geometry-dependent 3D chain alignment observed in this study.

CONCLUSION

In summary, the crystallization and chain alignment of P3HT by nanoimprint lithography are studied by GIXRD. We prove chain alignment is significantly impacted by geometry-dependent nanoconfinement during thermal nanoimprinting processes. The morphology and extent of chain ordering can be controlled by mold geometry as well as nanoimprint process conditions. The mechanism of ordering and alignment is proposed to be a combination of $\pi-\pi$ interchain interactions and side chain hydrophobic interactions with hydrophobic mold walls. The resulting P3HT nanostructures with vertical chain alignment have strong potential to improve charge transport and optical properties in both solar cell and FET applications alike. For example, $\pi-\pi$ stacking along the nanograting can enhance charge-carrier mobility for FETs, while the vertical chain alignment in nanopillars and nanogratings can enhance vertical charge transport in solar cells. At the same time, these nanostructures also provide vertically interdigitizing heterojunction morphology as demonstrated in our previous work.[20] We believe the demonstrated simultaneous control of P3HT nanomorphology and vertical chain alignment holds great potential to improve efficiency of organic solar cells using high-density interdigitized bicontinuous nanoheterojunction with ordered polymer chain alignment.

EXPERIMENTAL METHODS

A 1.5 wt % (17.55 mg/mL) portion of region-regular or RR-P3HT (Reike Metals Inc.) solution was prepared in chlorobenzene. The solution was filtered with 0.22 μm PTFE filter. P-type (100) Si was cleaned with acetone and isopropyl alcohol. An 80 nm thick P3HT film was then spincoated onto the Si substrates. The thicknesses of the thin film were measured with profilometer and confirmed in SEM. A grating mold of 65 nm width and 200 nm pitch and a nanoporous mold of hexagonal array of 80 nm wide nanopores with 100 nm pitch were used in the nanoimprint process. The detailed fabrication process of these molds was described elsewhere.[20] The molds were treated with FDTS as an antiadhesion coating. The nanoimprint was performed at a temperature of 170 °C and a pressure of 50 bar for 10 min. The system was cooled down slowly to room temperature, and the mold was released from the substrate. The nanostructures were characterized using SEM. GIXRD was carried out to measure the P3HT chain alignment on a Rigaku Ultima III diffractometer. Out-of-plane and in-plane GIXRD results were obtained. In the GIXRD experiments, the X-ray incident angle ω was fixed at 0.5° to the plane of sample surface during the scan. The angular spectrum was collected for 2θ ranging from 3° to 25°. For the prefer orientation ϕ scan measurement, the sample was placed on the thin film stage aligning the nanograting direction manually with the cross hair so that the nanograting becomes parallel to the incident beam when $\phi = 0°$, the scanning was done from $\phi = -40°$ to 115° with fixed detector at $2\theta = 5.2°$. The irradiation area of X-ray beam in GIXRD experiments is estimated as 15 mm × 5 mm, which is smaller than the imprinted samples (20 mm × 15 mm).

Acknowledgment. This work is supported by the National Science Foundation (No. ECCS-0901759) and the Air Force Office of Scientific Research (No. FA9550-06-1-0403).

REFERENCES AND NOTES

1. Gebeyehu, D.; Brabec, C. J.; Padinger, F.; Fromherz, T.; Hummelen, J. C.; Badt, D.; Schindler, H.; Sariciftci, N. S. The Interplay of Efficiency and Morphology in Photovoltaic Devices Based on Interpenetrating Networks of Conjugated Polymers with Fullerenes. *Synth. Met.* **2001**, *118*, 1–9.
2. Hoppe, H.; Sariciftci, N. S. Organic Solar Cells: An Overview. *J. Mater. Res.* **2004**, *19*, 1924–1945.
3. Friend, R. H.; Gymer, R. W.; Holmes, A. B.; Burroughes, J. H.; Marks, R. N.; Taliani, C.; Bradley, D. D. C.; Dos Santos, D. A.; Bredas, J. L.; Logdlund, M.; *et al*. Electroluminescence in Conjugated Polymers. *Nature* **1999**, *397*, 121–128.
4. Ong, B. S.; Wu, Y. L.; Liu, P.; Gardner, S. High-Performance Semiconducting Polythiophenes for Organic Thin-Film Transistors. *J. Am. Chem. Soc.* **2004**, *126*, 3378–3379.
5. Benanti, T. L.; Venkataraman, D. Organic Solar Cells: An Overview Focusing on Active Layer Morphology. *Photosynth. Res.* **2006**, *87*, 73–81.
6. Briseno, A. L.; Mannsfeld, S. C. B.; Jenekhe, S. A.; Bao, Z.; Xia, Y. Introducing Organic Nanowire Transistors. *Mater. Today* **2008**, *11*, 38–47.
7. Gustafsson, G.; Inganas, O.; Stafstrom, S. Optical Anisotropy of Neutral and Doped Poly(3-Octylthiophene). *Solid State Commun.* **1990**, *76*, 203–208.
8. Sirringhaus, H.; Brown, P. J.; Friend, R. H.; Nielsen, M. M.; Bechgaard, K.; Langeveld-Voss, B. M. W.; Spiering, A. J. H.; Janssen, R. A. J.; Meijer, E. W.; Herwig, P.; *et al*. Two-Dimensional Charge Transport in Self-Organized, High-Mobility Conjugated Polymers. *Nature* **1999**, *401*, 685–688.
9. Sirringhaus, H.; Wilson, R. J.; Friend, R. H.; Inbasekaran, M.; Wu, W.; Woo, E. P.; Grell, M.; Bradley, D. D. C. Mobility Enhancement in Conjugated Polymer Field-Effect Transistors through Chain Alignment in a Liquid-Crystalline Phase. *Appl. Phys. Lett.* **2000**, *77*, 406–408.
10. Comoretto, D.; Dellepiane, G.; Marabelli, F.; Cornil, J.; dos Santos, D. A.; Bredas, J. L.; Moses, D. Optical Constants of Highly Stretch-Oriented Poly(*P*-phenylene-vinylene): A Joint Experimental and Theoretical Study. *Phys. Rev. B* **2000**, *62*, 10173–10184.
11. Svensson, M.; Zhang, F.; Inganas, O.; Andersson, M. R. Synthesis and Properties of Alternating Polyfluorene Copolymers with Redshifted Absorption for Use in Solar Cells. *Synth. Met.* **2003**, *135*, 137–138.
12. Bassett, D. C., *Principles of Polymer Morphology*, Illustrated ed.; Cambridge University Press: New York, 1981; pp 146–166.
13. DeLongchamp, D. M.; Vogel, B. M.; Jung, Y.; Gurau, M. C.; Richter, C. A.; Kirillov, O. A.; Obrzut, J.; Fischer, D. A.; Sambasivan, S.; Richter, L. J.; *et al*. Variations in Semiconducting Polymer Microstructure and Hole Mobility with Spin-Coating Speed. *Chem. Mater.* **2005**, *17*, 5610–5612.
14. Kim, D. H.; Jang, Y.; Park, Y. D.; Cho, K. Controlled One-Dimensional Nanostructures in Poly(3-hexylthiophene) Thin Film for High-Performance Organic Field-Effect Transistors. *J. Phys. Chem. B* **2006**, *110*, 15763–15768.
15. Kline, R. J.; McGehee, M. D.; Toney, M. F. Highly Oriented Crystals at the Buried Interface in Polythiophene Thin-Film Transistors. *Nat. Mater.* **2006**, *5*, 222–228.
16. Chang, J. F.; Sun, B. Q.; Breiby, D. W.; Nielsen, M. M.; Solling, T. I.; Giles, M.; McCulloch, I.; Sirringhaus, H. Enhanced Mobility Of Poly(3-hexylthiophene) Transistors by Spin-Coating from High-Boiling-Point Solvents. *Chem. Mater.* **2004**, *16*, 4772–4776.
17. Heil, H.; Finnberg, T.; von Malm, N.; Schmechel, R.; von Seggern, H. The Influence of Mechanical Rubbing on the Field-Effect Mobility in Polyhexylthiophene. *J. Appl. Phys.* **2003**, *93*, 1636–1641.
18. Nagamatsu, S.; Takashima, W.; Kaneto, K.; Yoshida, Y.; Tanigaki, N.; Yase, K. Backbone Arrangement in "Friction-Transferred" Regioregular Poly(3-alkylthiophene)S. *Macromolecules* **2003**, *36*, 5252–5257.
19. Li, D.; Xia, Y. N. Electrospinning of Nanofibers: Reinventing the Wheel. *Adv. Mater.* **2004**, *16*, 1151–1170.
20. Aryal, M.; Buyukserin, F.; Mielczarek, K.; Zhao, X. M.; Gao, J. M.; Zakhidov, A.; Hu, W. C. Imprinted Large-Scale High Density Polymer Nanopillars for Organic Solar Cells. *J. Vac. Sci. Technol., B* **2008**, *26*, 2562–2566.
21. Cheyns, D.; Vasseur, K.; Rolin, C.; Genoe, J.; Poortmans, J.; Heremans, P. Nanoimprinted Semiconducting Polymer Films with 50 nm Features and their Application to Organic Heterojunction Solar Cells. *Nanotechnology* **2008**, *19*, 424016–414021.
22. Cui, D.; Li, H.; Park, H.; Cheng, X. Improving Organic Thin-Film Transistor Performance by Nanoimprint-Induced Chain Ordering. *J. Vac. Sci. Technol., B* **2008**, *26*, 2404–2409.
23. Kim, M. S.; Kim, J. S.; Cho, J. C.; Shtein, M.; Guo, L. J.; Kim, J. Flexible Conjugated Polymer Photovoltaic Cells with Controlled Heterojunctions Fabricated Using Nanoimprint Lithography. *Appl. Phys. Lett.* **2007**, *90*, 123113–123115.
24. Yazawa, K.; Inoue, Y.; Yamamoto, T.; Asakawa, N. Twist Glass Transition in Regioregulated Poly(3-alkylthiophene). *Phys. Rev. B* **2006**, *74*, 094204–094215.
25. Yang, C.; Orfino, F. P.; Holdcroft, S. A Phenomenological Model for Predicting Thermochromism of Regioregular and Nonregioregular Poly(3-alkylthiophenes). *Macromolecules* **1996**, *29*, 6510–6517.
26. Zhao, Y.; Yuan, G. X.; Roche, P.; Leclerc, M. A Calorimetric Study of the Phase-Transitions in Poly(3-hexylthiophene). *Polymer* **1995**, *36*, 2211–2214.
27. Beck, V. A.; Shaqfeh, E. S. G. Ergodicity-Breaking and the Unraveling Dynamics of a Polymer in Linear and Nonlinear Extensional Flows. *J. Rheol.* **2007**, *51*, 561–574.
28. Checker, N.; Mackley, M. R.; Mead, D. W. On the Flow of Molten Polymer into, within, and out of Ducts. *Phil. Trans. R. Soc., A (London)* **1983**, *308*, 451–477.
29. Rowland, H. D.; King, W. P.; Pethica, J. B.; Cross, G. L. W. Molecular Confinement Accelerates Deformation of Entangled Polymers During Squeeze Flow. *Science* **2008**, *322*, 720–724.
30. Lovinger, A. J.; Davis, D. D. Electron-Microscopic Investigation of the Morphology of a Melt-Crystallized Polyaryletherketone. *J. Appl. Phys.* **1985**, *58*, 2843–2853.
31. Kanazawa, H.; Stejny, J.; Keller, A. Polymerization and Structure of Poly(sulfur nitride) Prepared under High-Pressure. *J. Mater. Sci.* **1991**, *26*, 1635–1639.
32. Yamamoto, K.; Ochiai, S.; Wang, X.; Uchida, Y.; Kojima, K.; Ohashi, A.; Mizutani, T. Evaluation of Molecular Orientation and Alignment of Poly(3-hexylthiophene) on Au (111) and on Poly(4-vinylphenol) Surfaces. *Thin Solid Films* **2008**, *516*, 2695–2699.
33. Sandberg, H. G. O.; Frey, G. L.; Shkunov, M. N.; Sirringhaus, H.; Friend, R. H.; Nielsen, M. M.; Kumpf, C. Ultrathin Regioregular Poly(3-hexyl thiophene) Field-Effect Transistors. *Langmuir* **2002**, *18*, 10176–10182.
34. Hu, Z. J.; Muls, B.; Gence, L.; Serban, D. A.; Hofkens, J.; Melinte, S.; Nysten, B.; Demoustier-Champagne, S.; Jonas, A. M. High-Throughput Fabrication of Organic Nanowire Devices with Preferential Internal Alignment and Improved Performance. *Nano Lett.* **2007**, *7*, 3639–3644.